**Title:** Melt electrospinning writing of poly-hydroxymethylglycolide-co-ε-caprolactone-based scaffolds for cardiac tissue engineering

Miguel Castilho*, Dries Feyen, María Flandes-Iparraguirre, Gernot Hochleitner, Jürgen Groll, Pieter A.F. Doevendans, Tina Vermonden, Keita Ito, Joost P.G. Sluijter* and Jos Malda*

*Corresponding Author*

Dr. M. Castilho, Ms. María Flandes-Iparraguirre, Prof. K. Ito, Dr. J. Malda

Department of Orthopaedics

University Medical Center Utrecht

P.O. Box 85500, 3508  GA Utrecht , The Netherlands

E-mail: J.Malda@umcutrecht.nl

E-mail: M.DiasCastilho@umcutrecht.nl

Dr. Dries Feyen, Ms. María Flandes-Iparraguirre, Prof. Dr. Joost Sluijter, Prof. Dr. Pieter A.F. Doevendans

Department of Cardiology, Experimental Cardiology Laboratory

University Medical Center Utrecht

P.O. Box 85500, 3508 GA Utrecht , The Netherlands

E-mail:  J.Sluijter@umcutrecht.nl

Mr. G. Hochleitner, Prof. J. Groll

Department of Functional Materials in Medicine and Dentistry and Bavarian Polymer Institute

University of Würzburg

Pleicherwall 2, 97070 , Würzburg , Germany


Dr. T. Vermonden

Utrecht Institute for Pharmaceutical Sciences (UIPS)

Department of Pharmaceutics

Utrecht University

P. O. Box 80082, 3508 TB Utrecht, The Netherlands


Prof. K. Ito, Dr. M. Castilho

Department of Biomedical Engineering

Eindhoven University of Technology

P. O. Box 513, 5600 MB Eindhoven, The Netherlands


Dr. M. Castilho, Ms. María Flandes-Iparraguirre, Dr. Dries Feyen, Prof. Dr. Joost Sluijter, Dr. J. Malda

Regenerative Medicine Center Utrecht

Uppsalalaan 8, 3584 CT Utrecht, The Netherlands

**Abstract:** Current limitations in cardiac tissue engineering revolve around the inability to fully recapitulate the structural organization and mechanical environment of native cardiac tissue. In the current study, we aimed at developing organized ultra-fine fibre scaffolds with improved biocompatibility and architecture in comparison to the traditional fibre scaffolds obtained by solution electrospinning. This was achieved by combining the additive manufacturing of a hydroxyl functionalized polyester (poly(hydroxymethylglycolide-co-ε-caprolactone), pHMGCL) with melt electrospinning writing (MEW). The use of pHMGCL with MEW vastly improved the cellular response to the mechanical anisotropy. Cardiac progenitor cells (CPCs) were able to align more efficiently along the preferential direction of the melt-electropun pHMGCL-fibre scaffolds in comparison to electrospun poly(ε-caprolactone)-based scaffolds. Overall, this study describes for the first time that highly ordered microfibre (4.0-7.0 μm) scaffolds based on pHMGCL can be reproducibly generated with MEW and that these scaffolds can support and guide the growth of cardiac progenitor cells and thereby potentially enhance their therapeutic potential.

# 1. Introduction

Heart failure is a debilitating disease for patients and is often associated with a poor quality of life, as well as high morbidity and mortality (1). The heart is hardly able to repair after cardiac injury (*e.g.* due to myocardial infraction (MI)) and is often associated with progressive pathological remodelling to compensate for contractility loss (1). Current clinical therapies for heart failure do not treat the underlying loss of myocardial tissue, and thereby do not halt the progression of the disease. Therefore, regenerative therapies that involve stem or progenitor cells have been proposed as potential future approaches (2). Biomaterials have been suggested to be essential and useful as critical regulators of the organisation of stem cells for cardiac tissue engineering (TE) applications (3). Nonetheless, recreating native cardiac tissue *in vitro* still remains a major challenge (4, 5). Despite the great potential of 3D-biofabrication to accurately deposit cells and biomaterials together into desired geometries (6), these techniques are currently unable to fully address the needed structural fibre organization and mechanical environment of endogenous cardiac tissue.

In that respect, embedding cardiac progenitor cells into fibre-based scaffolds is a promising approach as the fibre network has the potential to mimic the fibrillar structure of the native extracellular matrix (ECM) (7). Amongst the different technologies used for fibre scaffold fabrication, electrospinning of polymer solutions is relatively popular due to its simplicity and cost-effectiveness. Recently, the potential of using electrospun fibre scaffolds of polycaprolactone (PCL) (8) or functionalized PCL to mimic the aligned ECM of the native heart muscle (9) was demonstrated. Nevertheless, the lack of biological compatibility of PCL compared to that of natural polymers necessitated post-processing steps in order to improve cell-scaffold interactions. Moreover, despite the promising micro-fibre diameters obtained,

appropriate fibre alignment and mechanical properties that could recreate the microenvironment of the cardiac tissue could not be achieved.

Direct melt electrospinning writing (MEW) is an additive manufacturing process that has recently emerged as an alternative polymer processing technology for fibre scaffold manufacturing (10). This technology is based on an electrohydrodynamic working principle to deposit fibres from polymer melts to highly defined scaffold structures. While the fibre diameters can be tailored between ~0.8 µm (11) and ~140 µm (12) depending on printing conditions and polymer characteristics, the range of polymers that have been applied in MEW is still very limited, with PCL being the most commonly used (13). However, PCL is relatively hydrophobic, degrades slowly and is, therefore, in our opinion not regarded as the ideal material for true myocardial integration and regeneration.

In the current study, we developed ultra-fine fibre scaffolds with enhanced biocompatibility and improved fibre architecture that could stimulate cell retention and guide cardiac cell growth. This was achieved by combining MEW technology with poly (hydroxymethylglycolide-co-ε-caprolactone) (pHMGCL) (Figure 1). This hydroxyl-functionalized polyester (pHMGCL) has increased hydrophilicity in comparison to PCL (14, 15), a tunable degradation rate and has the potential for further functionalization (16,17). Therefore, in this study MEW of pHMGCL was systematically investigated in order to obtain reproducible fibre scaffolds. Different scaffold architectures were compared to assess the effect on mechanical behaviour, cellular alignment and organisation. Biological relevance of the fibre scaffolds was tested with human cardiac progenitor cells (CPCs), a promising therapeutic cell type that can be isolated directly from a patients' heart and differentiated into cardiomyocytes and vascular cells (18).

## 2. Results and discussion

### 2.1. MEW

*2.1.1. Polymer characterization for melt electrospinning*

The ability to melt electrospin a polymer is mainly determined by material characteristics like molecular weight and thermal properties of the polymer (13). In this study, two polymer formulations were used, *i.e.* pHMGCL, PCL, and blends of pHMGCL with PCL in two different weight ratios (*i.e.* 20:80 – Blend20 and 40:60 – Blend40; material properties are summarized in Table 1). GPC analysis revealed that the molecular weight of pHMGCL ($M_w$=39 kDa) was substantially lower than that of PCL ($M_w$=71 kDa), while thermograms demonstrated a lower melting temperature of pHMGCL ($T_m$=44.5°C) when compared to PCL ($T_m$=54.4°C). By increasing the relative amount of pHMGCL from 20 to 40 wt%, the melting temperature of the blends slightly decreased in comparison with the pure PCL polymer. Hydrophilicity of the pHMGCL polymer and its blends was also confirmed by contact angle measurements, where pHMGCL had a much lower contact angle (54.2 ± 0.9°) than the PCL polymer alone (70.9± 1.5°), as reported previously (14). Consistently, measured contact angles for the 20 and 40 wt% pHMGCL blends were lower than for the pure PCL (67.2 ± 1.6° and 58.7 ± 2.1°, respectively). This underscores the potential of blending the PCL with pHMGCL to reduce the intrinsic hydrophobicity of the PCL polymer, without significant modification of its thermal properties.

*2.1.2 Fabrication of melt electrospun scaffolds*

Preliminary tests demonstrated that melt electrospinning of pHMGCL polymer resulted in a persistent non-continuous and unstable material jet despite the similar thermal properties to PCL, hampering the adequate material collection and writing (data not shown). This was most likely due to Rayleigh instabilities and consequently formation of non-continuous polymer jets due to the significantly lower $M_w$ and insufficient macromolecular entanglements of this

polymer compared to the PCL. On the other hand, the melt electrospinning of 20 wt% pHMGCL/PCL (Blend20) and 40 wt% pHMGCL/PCL (Blend40) yielded jets that enabled the direct-writing of fibres. As a superior interaction of the CPCs was expected for the Blend40 due to the higher hydrophilicity, this blend was specifically used for further evaluation. The interdependence of fibre properties on instrument parameters was subsequently evaluated in order to establish appropriate processing conditions.

*Investigation of processing parameters on fibre shape and diameter*

Polymer jet formation and dependency of fibre-shape on the velocity of the collector plate was examined for the Blend40 and PCL formulations (Figure 2). Continuous jets were formed between the Taylor cone and the contact point on the translating collector plate for both polymers. A slightly lower meniscus formation was observed at the nozzle end for the Blend40, as well as a lower jet deflection, when compared to the PCL polymer (selected representative images of polymer jet formation in Figure 2). Transition of sinusoidal fibres to straight fibres occurred at higher collecting speeds for the Blend40 (25 mm/s) than for the PCL (10 mm/s). This speed is usually defined as the 'critical translation speed' (CTS) (12) and defines the speed at which the collector plate matches the ultimate jet speed, which is critical for the fabrication of scaffolds with well-defined and controlled architectures (Figure 2).

Having determined the CTS for both polymer formulations, the effect of the key processing parameters *i.e.* feeding pressure (p), applied voltage ($U_{acc}$), collecting speed ($v_{col}$) and collecting distance (d) on fibre diameter was systematically investigated (Figure 2 c - e). By increasing the feeding pressure from 1 to 4 bar, the average diameter of the deposited fibres increased from approximately 3 µm to 7 µm and 4 µm to 12 µm for the Blend40 and PCL, respectively. This increased diameter can be explained by the increase in molten polymer flow rate and was more pronounced for the PCL polymer. With the increase of the applied voltage a jet-thinning effect

was observed (Figure 2 d). This phenomenon is in line with observations reported previously for fibre fabrication with both solution (19) and melt-electrospinning (20). Moreover, the diameter of the fibres decreased, regardless of polymer composition, approximately with 40% when the collector translational speed was doubled. This latter instrument parameter mostly dictates the mechanical drawing forces and, therefore, was found to also play a critical role in controlling both fibre shape and diameter. In addition, the effect of collector distance on fibre diameter was studied but no clear effect was observed (data not shown). This might be related to the fact that only at spinning distances of 3 to 5 mm stable jets were observed. Finally, the spinning temperatures were kept at the minimum spinning temperatures for stable printing conditions: 87°C and 94°C for Blend40 and PCL, respectively. This was higher than the determined melting temperatures (as determined by DSC analysis) due to an energy loss observed through MEW printing head and also to ensure a sufficient drop in the viscosity of the molten polymers, required to attain stable polymer jets. Thus, melt electrospinning of the Blend40 was found to require considerable higher acceleration voltages, $U_{acc} = 7$ kV, higher collecting speeds, $V_{col} = 25$ mm/s and lower spinning temperatures, T= 84 °C, than the standard PCL polymer, in order to generate fibres with a diameter of approximately 4-7 µm. The fibre diameters obtained from the pHMGCL containing blends were close to the lowest fibre diameters typically obtained for MEW of PCL, 0.8 µm - 60 µm (8, 9, 21), and one order of magnitude lower than the common extruded 3D-printed PCL scaffolds (22). Such fibre diameters of 4-7 µm were chosen as these provide a good balance between cellular interaction and scaffold handling. With regards to optimal cell adhesion, thin fibres are often preferred due to the high specific surface area (23). However, scaffolds with fibres below 3-5 µm were hard to handle and may be more prone to loss of their structural stability during *in-vivo* application.

*Layer-by-layer deposition: Scaffold manufacturing*

In order to create coherent 3D scaffold structures with relevant pore sizes for cardiac TE, the ability to stack micro fibres in a layer-by-layer fashion was evaluated. SEM analysis revealed the accurateness of the fibre stacking for the two types of scaffold geometries, *i.e.* rectangular and squared, from both polymers, Blend40 and PCL (Figure 3). Linear fibres were successfully stacked on the top of each other up to a height of 400 μm, comparable to a 3D-printed heart patch previously implanted in a murine model of myocardial infarction (3). Furthermore, the minimum pore size (*i.e.* interfibre distance) was approximately ±150 μm, without significant differences between the two polymer formulations. For interfibre distances below 150 μm, unstable jets were observed due to the repulsive forces generated between deposited fibres and the polymer jet (10). Therefore, the squared and rectangular shaped scaffolds were printed with the side dimensions of 200 x 200 μm and 150 x 300 μm, respectively. Aside from the small pore size achieved with a periodic structure, voids between adjacent fibres were observed at the edges of the box-structures (arrow in Figure 3c). These pores through the walls of stacked fibres were observed for both Blend40 and PCL scaffolds and were most likely determined by the differences in the cumulative charge of each fibre stack that repelled the subsequent layer or due to an heterogenous tensile drag (24).

## 2.2 Mechanical testing of the MEW fibrous scaffolds

Mechanical properties of the MEW fibrous scaffolds were evaluated under uniaxial tensile loading conditions (Figure 4) and a non-linear stress-strain behaviour was observed for all scaffolds. When comparing the modulus of the rectangular shaped scaffolds in direction 1 (short axis) to direction 2 (long axis), a significant increase from $0.70 \pm 0.15$ to $1.46 \pm 0.14$ MPa and from $1.18 \pm 0.08$ to $2.05 \pm 0.15$ MPa was observed for the Blend40 and PCL scaffolds, respectively (Figure 4d). For the square shaped scaffolds, no significant difference was

observed between the modulus in direction 1 and 2, yielding values from 1.94 ± 0.12 to 2.10 ± 0.14 MPa and 2.40 ± 0.10 to 2.25 ± 0.42 MPa for the Blend40 and PCL scaffolds, respectively. In all cases, the tensile modulus for the Blend40 scaffolds was lower than the correspondent PCL based scaffolds. This difference likely resulted from the shorter polymer chains of pHMGCL when compared to the PCL polymer. Despite of the relatively inferior tensile properties of the pHMGCL based scaffolds, the tensile modulus of both polymers is close to the range of stiffnessess reported in the literature for human myocardium (25). To investigate further, the ratio between the tensile modulus in both testing directions was determined for all constructs (Figure 4 e). As predicted, the rectangular shaped scaffolds of both polymer formulations evidenced anisotropic behaviour ($E_{T2}/E_{T1} \approx 2$), whilst the squared ones showed a more isotropic behaviour ($E_{T2}/E_{T1} \approx 1$). The aligned fibre scaffolds with a rectangular shape were then found to successfully approximate not only the effective stiffness but also the anisotropic behaviour of the native heart tissue (25, 26). It should be noted that only the short-term mechanical properties were evaluated at this stage and also, it was not evaluated whether these novel constructs interfere with the mechanical functioning of the native tissue surrounding the graft after myocardium implantation.

**2.3 Biological performance**

*2.3.1 Cell encapsulation and viability*

To investigate the biological performance, CPCs were combined with a collagen hydrogel and seeded into both the Blend40 and PCL scaffolds. After 7 days, cells were uniformly distributed inside the scaffold, as shown by immunostainings for F-actin and integrin-β1 (Figure 5), with CPCs dispersed throughout the pores and in close contact with the fibres. Cell viability in the scaffolds was assessed with a live-dead staining after 7 days of culture (Figure 5A). In Blend40 scaffolds, very few dead cells were detected with an estimated survival rate of 99.9% and with

no distinction seen between the different geometries. In the case of PCL scaffolds the cell survival rate was also high with an estimated survival rate of around 98%. The high observed cell viability with both material was to be expected, given the fact that the PCL is already widely used successfully in medical application (27), and Blend40 is designed as a more cell friendly alternative. A control group of CPCs combined with only the collagen hydrogel was also prepared. However, without the support of the fibre scaffolds CPCs completely remodelled the collagen matrix into a small clump of tissue within the first 24hours. Therefore, this group was not included for further cell alignment evaluation.

*2.3.2 Cell alignment*

The analysis of the nuclear alignment angle and circularity revealed an influence of the scaffold architecture in the cellular arrangement. The squared geometry resulted in a completely isotropic cellular distribution, with the cells randomly arranged in all directions (Figure 5). The scaffolds with a rectangular architecture, on the other hand, promoted cellular alignment in the preferential direction of the fibres, $E_2$ (rectangle long axis). Moreover, it was observed that 50% of the cells aligned within 20º in the case of PCL, whilst 65% of the cells aligned in the Blend40 scaffolds. These results demonstrated a statistical significant difference in cellular alignment between the Blend40 and PCL scaffolds. Similar outcomes were found in the nuclear shape index (NSI), for which CPCs nucleus in the rectangular Blend40 scaffolds were less circular compared to their squared counterparts. It is noteworthy to mention that nuclear alignment can be seen even in the cells far from the fibres (see Figure 5), suggesting that, even though cells sense the fibres at a local level, the Blend40 scaffolds promote organization on a macroscopic scale. Furthermore, CPCs homogenous distribution and alignment throughout the scaffold thickness was confirmed by serial confocal sections at 4 different depths of a squared PCL scaffold (Supplementary Figure 1).

Whereas previous studies have reported limited cell infiltration in fibre scaffolds created by electrospinning ( 28 ), our MEW scaffolds showed a highly porous structure with fully interconnected porosities. The presence of porosity through scaffold walls enabled all compartments to interact (Figure 3C), thereby likely improving CPC cell communication and migration. Nevertheless, these pores show not a clear homogeneity and are not adequately distributed over the scaffold walls. Future studies should address more uniform pore generation within the walls of the fibre scaffolds without compromising accurateness of the fibre stacking. Moreover, the conductivity of the pHMGCL fibres may be improved to allow electrical stimulation as this has been shown to positively influence CPC's behavior (29). Furthermore, electrical stimulation is suggested for further maturation of potential constructs and to improve the conductance over the construct for the propagation of electrical signals between adjacent cells, especially with the use of contractile cardiomyocytes.

## 3. Conclusion

In summary, cardiac scaffolds with highly organized fibre architectures were successfully produced by MEW of pHMGCL/PCL blends for the first time. Constructs having a rectangular pattern were found to approximate to the broad mechanical properties of the native myocardial tissue, while, at the same time, promoting CPCs alignment according to the rectangular shape scaffold long-axis. Furthermore, the utilization of pHMGCL-based polymer provided a higher degree of cellular alignment in comparison with commonly used PCL polyester. Thus, we envision that our developed approach with enhance cardiac mechanical and biological relevance can provide a framework for the development of therapeutic viable *in vitro* cardiac engineered tissues.

**Experimental Section**

*Materials:* PCL (PURASORB PC 12, Gorinchem, Netherlands) was purchased from Corbion. pHMGCL, was prepared according to the method previously described by Seyednejad *et al.* (14). Briefly, this hydroxyl functionalized polyester was synthesized via ring opening polymerization of 3S-benzyloxymethyl-1,4-dioxane-2,5-dione (benzyl protected hydroxymethyl glycolide (BMG)) and ε-caprolactone (monomer to initiator molar ratio of 300/1) in the melt at 130°C for 16-24 h, using benzyl alcohol (BnOH) and stannous octoate (SnOct$_2$) as initiator and catalyst, respectively. Synthesized polymer was then deprotected to yield the pHMGCL. Blends of pHMGCL/ PCL were prepared by mixing both components in a 20:80 and 40:60 weight ratio, and subsequently dissolved in dichloromethane (DCM), to uniformly disperse the two polymers. The solution was stirred at room temperature for 15 min and then the DCM was allowed to evaporate overnight under a flow of dry air. After complete DCM evaporation, solid polymer blends were stored at low temperatures (-5°C). The chemical structure of the prepared pHMGCL/PCL blends is shown in supplementary Figure 2.

*Materials characterization:* Molecular weights of the raw polymers were measured by gel permeation chromatography (GPC) on a 2695 Waters Alliance system and a Waters 2414 refractive index detector. Polystyrene standards of known molecular weights were used as standards using AR grade THF as eluent, at the operating conditions of 1 mL/min and 30 °C. The concentration of the polymers was 5ml/ml and injection volume was 50μL. Thermal properties of the raw polymers and blends were analyzed by Differential Scanning Calorimetry (DSC) on a DSC Q2000 apparatus (TA Instruments, DE, USA). 5 mg of each polymer composition was loaded into an aluminum pan and scanned from -80°C to 100°C with a heating rate of 10°C/min and a cooling rate of 0.5°C/min, under nitrogen flow. Glass transition temperature ($T_g$), melting temperature ($T_m$) and heat of fusion ($\Delta H_f$) were determined. Changes

in polymer surface wettability were evaluated by static contact angle measurements using sessile drop technique (Data Physics, OCA 15EC). All measurements (n = 3) were performed on uniform polymer films of each composition with a water droplet of 10 µl and repeated in triplicate. Contact angles were measured by averaging the right and left angles of the water droplet using the surface contact angle software (SCA20, Data Physics).

*Melt Electrospinning Writing:* MEW was performed by a custom-made device as schematically represented in Figure 1. In brief, the device consisted of four principle modules: a dispensing unit, a heating system, an electric field circuit and a collection set-up. The dispensing module contained a disposable glass syringe where the raw polymers and blends were inserted, coupled to one end to a thin metallic nozzle (27G, Unimed Switzerland), and to the other end to a manual pressure regulator (Festo, Germany) operating with air. The heating module was composed of an electrical heating coil element wrapped around the glass syringe and directly connected to a proportional–integral–derivative controller (TR 400, HKEtec, Germany) to control the polymer melting temperature. The electric field was generated by a high voltage (HV) source (LNC 10000, Heinzinger® Power supplies, Rosenheim, Germany) between a positive output applied to the syringe nozzle and the grounded planar aluminum collector plate. The plate was driven by an x-y lead screw set-up (Xslide, Velmex, LG-Motion, UK) controlled via an advanced 2-axis stepper motor controller (PMX-2EX-SA, ARCUS Technology- Inc., USA).

*Parameters range:* Polymer processing compatibility was systematically investigated according to key MEW parameters specifically, the acceleration voltage ($U_{acc}$), the feeding pressure (p), the collector velocity ($v_{col}$) and the collection distance (d). Fibre diameter and morphology were investigated by changing the mentioned parameters for the following values: $U_{acc}$ = [5 , 8.5] kV, P = [1 , 4] bar, $v_{col}$ = [10 , 40] mm/s and d = [3 , 5] mm, one parameter at a time. Several single fibres were printed, at each parameter combination, on microscopic slides

placed onto the aluminum collector plate, and then examined using a polarized light microscopy (BX51P, Olympus, Japan). The number of fibres used for the diameter measurements was at least n = 20. Subsequently, pHMGCL based scaffolds were manufactured using the following MEW parameters: $U_{acc}$ = 5 kV, p = 2 bar, $v_{col}$ = 5 mm/s and d = 3 mm; whilst for the pure PCL scaffolds the parameters used were $U_{acc}$ = 7 kV, p = 3 bar, $v_{col}$ = 25 mm/s and d = 3 mm. As control, the real temperature at the MEW syringe was evaluated locally with an handheld thermometer.

Well-organized scaffold meshes (5 x 5 $cm^2$) having squared (200 x 200 µm) and rectangular patterns (150 x 300 µm) were programmed and fabricated. The final height of every scaffolds was set to approximately 400 µm, which conformed with 25-30 layers. During all printings, temperature and relative humidity were kept at 19 − 21°C (accuracy ± 1°C) and 35 - 40% (accuracy ± 5%), respectively. Printed scaffolds were then visualized using a scanning electron microscopy (SEM) Phenom Pro (Phenom-World, The Netherlands), at an acceleration voltage of 5 − 10 kV. Prior to scanning, circular samples with a diameter of 5 mm were cut from the MEW meshes and sputter-coated with a 2 nm layer using a Q150R rotary-pumped sputter (Quorum Technologies, UK). Based on the scaffolds SEM images the fibre diameter and inter-fibre spacing was measured by using ImageJ software.

*Mechanical properties:* The tensile properties of the fabricated MEW scaffolds were measured on a Q800 DMA (TA Instruments, USA). Tests were performed from 0.01 till 1 N at a constant rate of 0.1 N/min. Rectangular shaped samples (n=5) with a length of 10 mm ($L_0$) and a width of 7 mm ($w_0$) were cut from each scaffold mesh and attached to a card board to ensure a correct alignment and positioning in the tensile grips. The effective elastic modulus, $E_T$, was calculated from the engineering stress-strain curves at the linear region (*i.e.,* 0 − 3% strain region), using the following equation,

$$E_T = FL_0 / \Delta L \, w_0 n_L \mathnormal{\varnothing}_f$$

where F denotes the applied load, $\Delta L$ is the length variation, $n_L$ is the number of printed layers and $\mathnormal{\varnothing}_f$ is the fibre diameter. Electrospun scaffolds were tested according to the two directions of fibre deposition 1 and 2 (Figure 4). Their directional dependent mechanical behavior was quantified by determining the ratio between the effective modulus obtained in both testing directions.

*Cell expansion and combination with melt electrospun scaffolds:* Cylindrical scaffolds of 8 mm in diameter were punched from the electrospun meshes. Prior to cell incorporation, scaffolds were sterilized by soaking them in 70% ethanol for 20 minutes, followed by a 20 min exposure to ultraviolet light on each side. Human cardiac progenitor cells (CPCs) were obtained and cultured as previously described (30). To facilitate the cell seeding process, a custom-made mold was used to hold the scaffolds in place. CPCs were suspended in a collagen type I solution and infused into the different scaffolds (n = 3) at a concentration of $8 \times 10^6$ cells/ml. Collagen solution was prepared as following, 340 μl Collagen type I (Collagen I rat protein, Thermo Fisher Scientific), 500 μl 2x DMEM, 150 μl PBS and 10 μl 0.1 M NaOH to balance pH. Constructs were kept in culture for 7 days, after which the whole constructs were either used for a live/dead assay, or fixed in paraformaldehyde for 20 minutes and kept in PBS at 4ºC until further use.

*Cell viability:* The cell viability in the constructs was assessed at day 7 by using a live/dead staining (Live/dead Viability/cytotoxicity kit, Thermo Fisher Scientific, United States), carried out according to the manufacturer's instructions.

*Cell alignment:* In order to visualize the cell morphology, stainings for F-actin and integrin-β1 were performed. Briefly, after incubating a primary mouse monoclonal antibody for integrin-β1 (12G10, Santa Cruz Biotechnology, United States) overnight at 4ºC, secondary fluorescent

marker (Alexa-Fluor 555, Thermo Fisher Scientific, United States) was added and incubated for 1h. Afterwards, F-actin was stained using marked phalloidin (Fluorescein Phalloidin, Thermo Fisher Scientific, United States). Samples were counterstained with nuclear Hoechst dye for 5 min. Visualization of the samples was performed using a confocal microscope (Leica TCS SP8, Leica Microsystems, Germany) and the images obtained were analyzed using ImageJ software. Built-in functions of ImageJ were used to calculate the nuclear alignment angle and shape index, which were used as a quantitative measure of cell alignment, as previously reported (31, 32). The nuclear alignment angle is defined as the orientation of the major axis of the ellipse that better fits the individual nuclei, and is expressed hereby with respect to direction 2, which corresponds to the direction of the fibres aligned in the vertical direction (long axis of the rectangles, Figure 5). Cells arranged within 10º relative to direction 2 were considered to be aligned, as previously described (33). The nuclear shape index (NSI), also known as circularity, was chosen as a measure of the nuclear elongation and subsequently calculated as follows,

$$NSI = (Area \times 4 \times \pi)/Perimeter^2$$

with a value of 1 representing a perfect circular shape.

*Statistical analysis:* Statistical analysis of the mechanical parameters and cellular alignment was performed using one-way ANOVA post hoc test (Tukey´s test). Differences were considered significant at a probability of error (p) of $p < 0.05$. All data are represented as means ± standard deviations.

**Acknowledgements**

17

**Figures**



**Figure1:** a) Schematic of the custom-built MEW device and its principal components: Dispensing unit assisted by air-pressure; electrical heating system; HV source electrode; computer assisted collector plate. b) Produced melt electrospun fibre scaffolds based on pHMGCL polymer. Optical image of well-organized scaffolds architecture (microfibres Ø=4.0-7.0 µm) having a rectangular pattern (pore size = 150 x 300 µm). c) Fibre scaffold infiltrated with CPCs / Collagen hydrogel. Immunostaining of the rectangular scaffolds seeded after 7 days in culture, showing that the oriented fibre architecture promoted cell alignment according to the rectangular shape scaffold long axis. Nuclei: stained in blue.
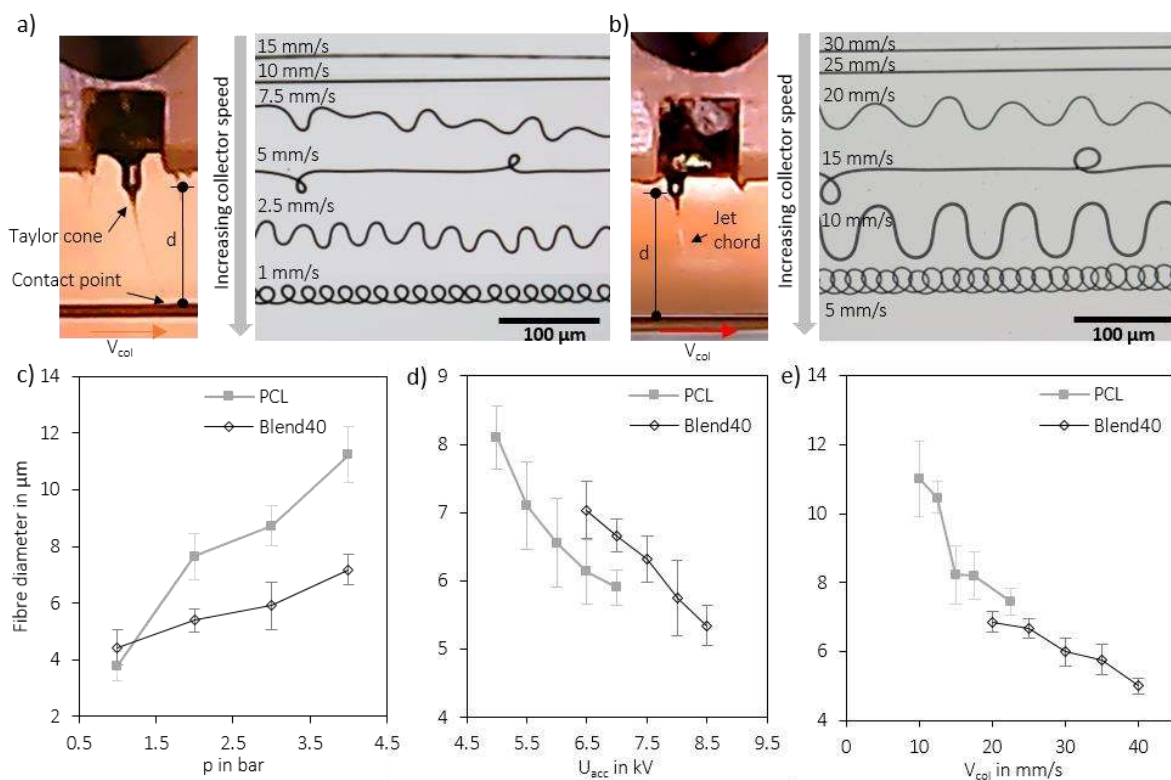
**Figure 2.** Effect of MEW key processing parameters on fibre shape, diameter and orientation. Optical micrographs of fibre shape modification at different collector speeds for a) PCL and b) Blend40. Stable segment of fibre jet formation between the Taylor cone and contact point on the subtract is also illustrated for both polymers at the collection distance of d = 3 mm. Evaluation of fibre diameter as function of c) feeding pressure (p), d) acceleration voltage ($U_{acc}$) and e) collector velocity ($v_{col}$) for the collection distance represented.
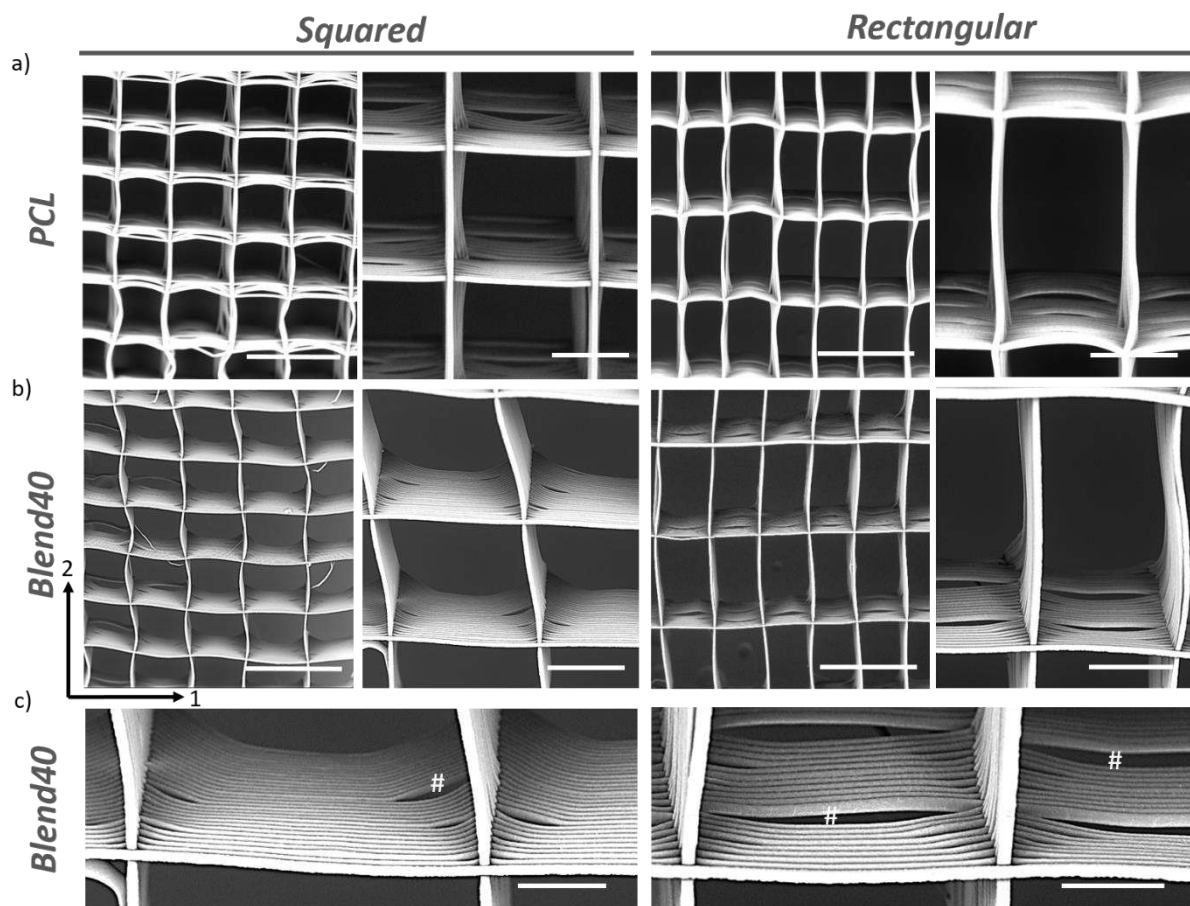
**Figure 3.** SEM images of the squared and rectangular MEW micro-fibrous scaffolds prepared from a) PCL and b) Blend40 polymer. Scaffolds were printed with 200 x 200 μm (squared) and 150 x 300 μm (rectangular) inter-fibre spacing and with a thickness of 400 μm (25 - 30 layers). Scale bars 300 μm (low magnification) and 100 μm (high magnification). c) Detailed view of the stacked fibres in Blend40 scaffolds. Local separation of the fibre stacks were observed, creating a porosity between the scaffold compartments (marked with #). A similar effect was observed for PCL scaffolds. Scale bar 50 μm.
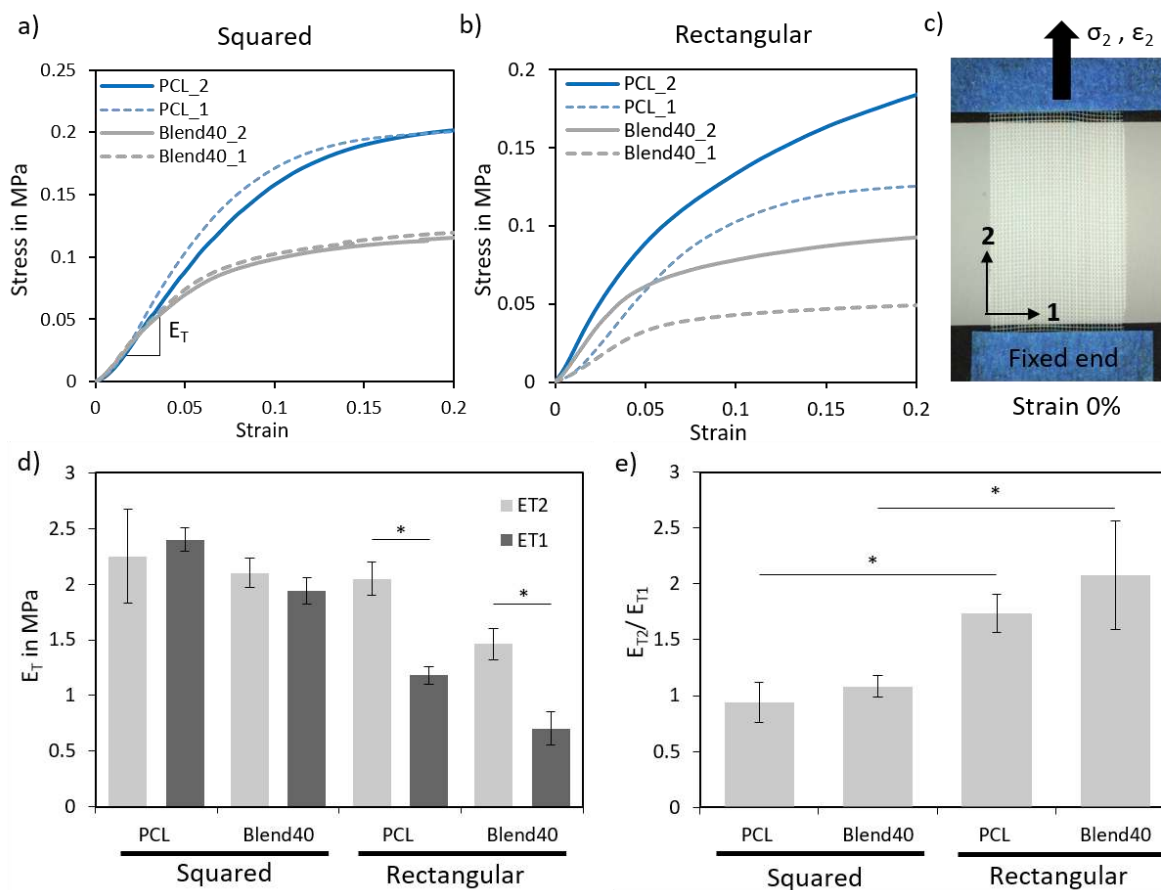
**Figure 4.** Mechanical properties of prepared MEW fibre scaffolds. Typical engineering stress–strain curve for a) squared and b) rectangular shaped scaffolds of PCL and Blend40 polymer, when tested under uniaxial tensile test according to the two printing directions, 1 and 2. C) Representative optical image of the sample geometry and fixation grips used for tensile tests. D) Comparison of d) tensile modulus ($E_T$) in both printing directions and e) tensile modulus ratio between both direction ($E_{T2}/E_{T1}$) of prepared scaffolds. A probability of error (p) of <0.05 is illustrated with *.
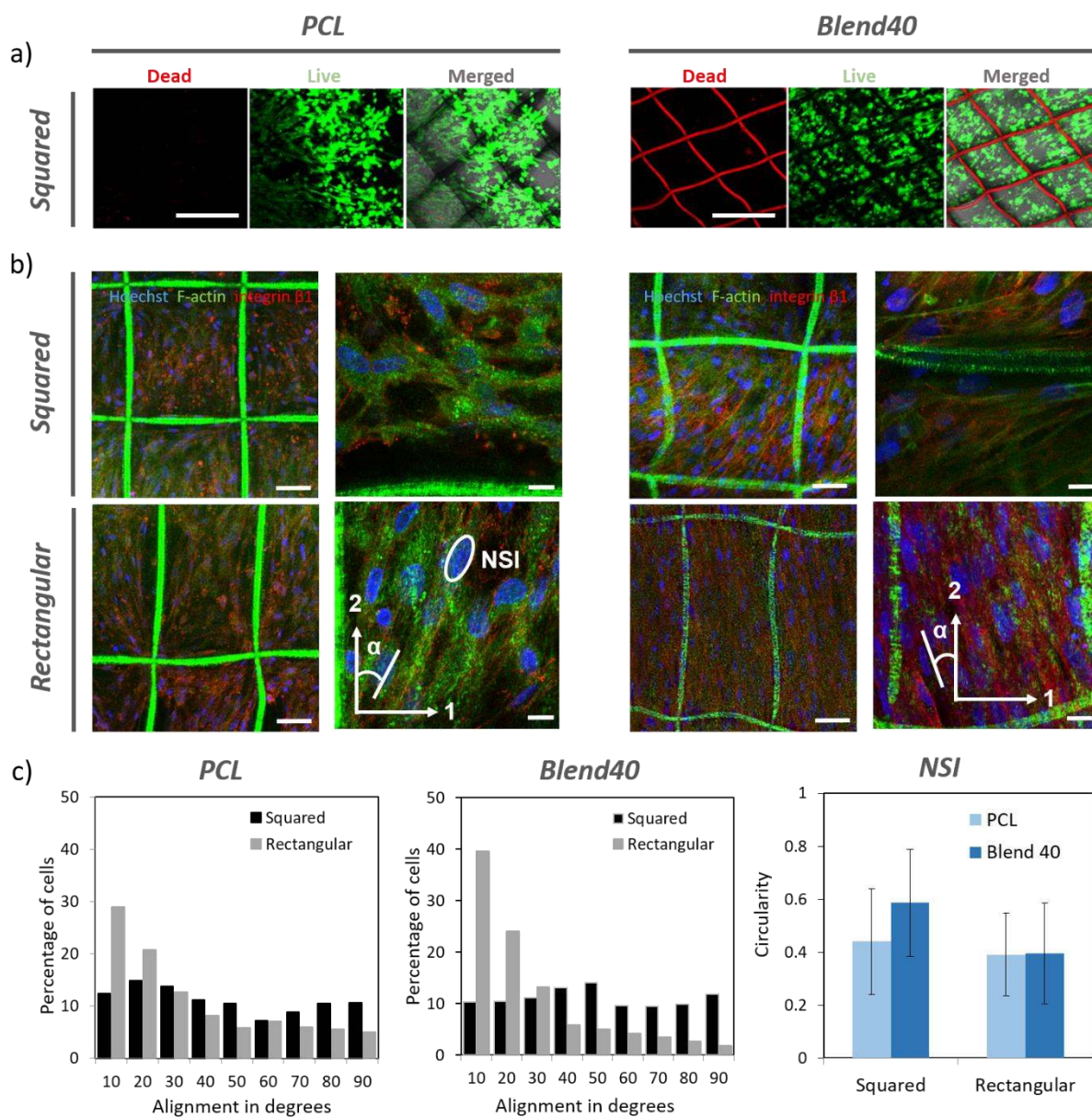
**Figure 5.** CPCs behavior on the fabricated MEW PCL and Blend40 / collagen composite fibrous scaffolds. a) Viability analysis of CPCs 7 days after embedding in PCL and Blend40 MEW scaffolds. In both conditions, seldom dead cells (red) were observed throughout the pores in the scaffold, with approximately 98-100% survival rate in all conditions. Scale bar is 250 µm. b) Confocal images of the constructs after 7 days in culture, stained with Hoechst (blue), F-actin (green) and integrin β1 (red). Scale bar for left images of each polymer composition is 50 µm, whereas for right images is 20 µm. c) Quantification of the CPC's alignment, α, on the

scaffolds. Alignment was measured with respect to the vertical micro fibres (direction 2), and assumed always positive. Nuclear shape index, NSI, variation as a measure of the circularity of the cell nuclei.

## Tables

**Table 1.** Characteristics of the pure polymers and blends used in this study.

| Composition | $M_w$ [kDa] [a] | PDI [a] | $T_g$ [°C] [b] | $T_m$ [°C] [b] | Water contact angle [°] | |
|---|---|---|---|---|---|---|
| PCL | 71 | 1.9 | -65.5 | 54.4 | 70.9±1.5 |  |
| pHMGCL | 38.9 | 2.1 | -51.6 | 44.5 | 54.2±0.9 |  |
| Blend20 | N.A | N.A | -60.4 | 54.1 | 67.2±1.6 |  |
| Blend40 | N.A | N.A | -59.2 | 54.2 | 58.7±2.1 |  |

Measured by [a] GPC; [b] DSC

## Supporting Information
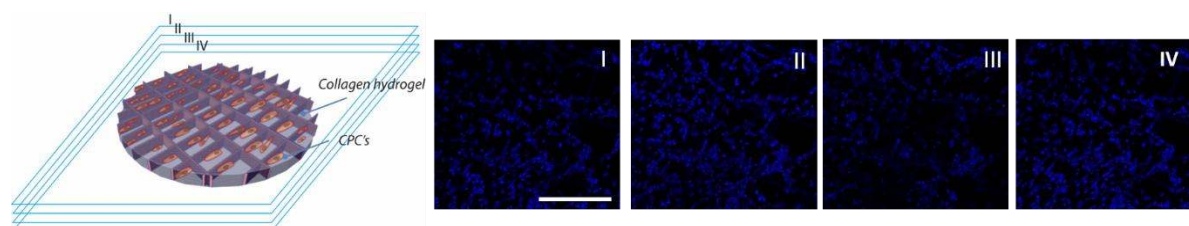


**Supplementary Figure 1:** Distribution of CPCs on a MEW PCL scaffold with a squared geometry. Serial confocal sections were taken at four different depths (every 80 μm) showing a homogeneous cell distribution throughout the scaffold thickness (400 μm). Cell nuclei were stained with Hoechst (blue). Scale bar is 250 μm.

Poly(hydroxymethylglycolide-co-ε-caprolactone), pHMGCL



Polycaprolactone, PCL
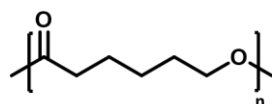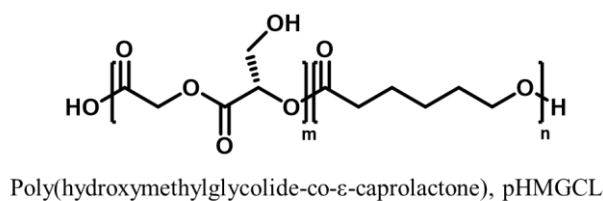
| Blend | Content in wt% | |
|---|---|---|
| | pHMGCL | PCL |
| Blend 20 | 20 | 80 |
| Blend 40 | 40 | 60 |

**Supplementary Figure 2**. Chemical structure of poly (hydroxymethyl glycolide-co-ε-caprolactone) (pHMGCL) and polycaprolactone (PCL) pure polymers and blends used in this study.

**References**

1 M. A. Laflamme, C.E. Murry **2011** *Nature* 473, 326-35. doi: 10.1038/nature10147.

2 D. A.M. Feyen, R. Gaetani, P.A. Doevendans P.A., J. P.G. Sluijter **2016** *Adv Drug Deliv Rev.* doi: 10.1016/j.addr.2016.04.023.

3 R. Madonna, L.W. Van Laake, S.M. Davidson, F.B. Engel, D.J. Hausenloy, S. Lecour, J. Leor, C Perrino, R. Schulz, K. Ytrehus, U. Landmesser, C. L. Mummery, S. Janssens, J. Willerson, T. Eschenhagen, P. Ferdinandy, J. P. Sluijter **2016** *Eur Heart J.* 37, 1789-98.

4 K. Zhu, S. Shin, T. Kempen, Y. Li, V. Ponraj, A. Nasajpour, S. Mandla, N. Hu, X. Liu, J. Leijten, Y. Lin, M. Asif Hussain, Y. Zhang, A. Tamayol, A. Khademhosseini **2017** *Adv. Funct. Mater.* 1605352.

5 R. Gaetani, D. A.M. Feyen, V. Verhage, R. Slaats, E. Messina, K. Christman, A. Giacomello, P. A.F.M Doevendans, J. P.G. Sluijter *Biomaterials* **2015**, 61, 339-348.

6 J. Groll, T. Boland, T. Blunk, J. A. Burdick, D. Cho, P. Dalton, B. Derby, G. Forgacs, Q. Li, V. A. Mironov, L. Moroni, M. Nakamura, W. Shu, S. Takeuchi, G. Vozzi, T. B. F. Woodfield, T. Xu, J. J. Yoo, J. Malda **2016** *Biofabrication* 8, 013001

7 M. Kitsara, O. Agbulut, D. Kontziampasis, Y. Chen, Philippe Menasché *Acta Biomaterialia* **2017,** 48, 20–40

8 D. Kai, M. Prabhakaran, G. Jin, S. Ramakrishna *J Biomed Mater Res B Appl Biomater.* **2011** 98, 379-86.

9 A. Guex, A. Frobert, J. Valentin, G. Fortunato, D. Hegemann, S. Cook, T. Carrel, H. Tevaearai, M. Giraud *Acta Biomaterialia* **2014**, 10, 2996–3006.

10 T. Brown, P. Dalton, D. Hutmacher *Advanced Materials* **2011**, 23, 5651–5657

11 G. Hochleitner, T Jungst, T. Brown, K. Hahn, C. Moseke, F. Jakob, P.D. Dalton, J. Groll *Biofabrication* **2015** 7 035002

12 G. Hochleitner, J.F. Hümmer, R. Luxenhofer, J Groll *Polymer* **2014**, 55, 5017-5023.

13 T. Brown, P. Dalton, D. Hutmacher *Prog. Polym. Sci.* **2016**, 56, 116–166

14 H. Seyednejad, T. Vermonden, N.E. Fedorovich, R. van Eijk, M.J. van Steenbergen, W.J Dhert, C.F. van Nostrum, W.E. Hennink, *Biomacromolecules* **2009**, 10, 3048-54.

15 H. Seyednejad, W. Ji, F. Yang, C. F. van Nostrum, T. Vermonden, J. van den Beucken, W. J.A. Dhert, W. E. Hennink, J. A. Jansen *Biomacromolecules* **2012,** 13, 3650–3660.

16 K. Boere, J. Visser, H. Seyednejad, S. Rahimian, D. Gawlitta, M. J. van Steenbergen, W. J.A. Dhert, W. E. Hennink, T. Vermonden, J. Malda, *Acta Biomaterialia* **2014**, 10, 6, 2602-2611

17 K. Boere, M. M. Blokzijl, J. Visser, J. E. Linssen, J. Malda, W. E. Hennink, T. Vermonden *J. Mater. Chem. B*, **2015**, 3, 9067.

18 M. J. Goumans, T. P. de Boer, A. M. Smits, L. W. van Laake, P. van Vliet, C. H. Metz, T. H. Korfage, K. P. Kats, R. Hochstenbach, G. Pasterkamp, M.C. Verhaar, M. A. van der Heyden, D. de Kleijn, C. L. Mummery, T. A. van Veen, J. P. Sluijter,P. A. Doevendans *Stem Cell Res.,* **2007** 1 138-49.

19 S-H. Tan, R. Inai, M. Kotaki, Ramakrishna, *Polymer* **2005,** 46, 6128-6134.

20 G. Hochleitner, A. Youssef, A. Hrynevich, N. Haigh Jodie, T. Jungst, J. Groll, P. Dalton *BioNanoMaterials* **2016** 10.1515/bnm-2015-0022.

21 T. Brown, A. Slotosch, L. Thibaudeau, A. Taubenberger, D. Loessner, C. Vaquette, P. Dalton, D. Hutmacher *Biointerphases* **2012,** 7, 1-16.

22 H. Kang, S. Jin Lee, I. Ko, C. Kengla, J. Yoo & A. Atala *Nature Biotechnology* **2016**, 34, 312–319.

23 F. Tian, H. Hosseinkhani, M. Hosseinkhani, A. Khademhosseini, Y. Yokoyama, G.G. Estrada, H. Kobayashi **2008** *Journal of Biomedical Materials Research Part A* 84(2) 291-299.

24 T. Brown, F. Edin, N. Detta, A. Skelton, D. Hutmacher, P. Dalton *Materials Science and Engineering: C* **2014**, 45, 698–708.

25 L. A. Reis, L. Chiu, N. Feric, L. Fu, M. Radisic *J. Tissue Eng. Regen Med.* **2016,** 10, 11-28.

26 Q. Chen, A. Bismarck, U. Hansen, S. Junaid, M. Tran, S. Harding, N. Ali, A. Boccaccini *Biomaterials* **2008,** 29, 47–57.

27 M. A. Woodruff, D. W. Hutmacher **2010** Progress in Polymer Science 35, 1217-1256

28 M.F. Leong, WY Chan, KS Chian, MZ Rasheed MZ, JM Anderson *J Biomed Mater Res A.* **2010** 94 (4):1141-9

29 S. Fleischer, M. Shevach, R. Feiner, T. Dvir 2014 Nanoscale 6 9410–4. doi:10.1039/c4nr00300d.

30 A. M Smits, P. van Vliet, C. H. Metz, T. Korfage, J. P. Sluijter, P. A. Doevendans, & M. J. Goumans **2009** *Nat Protoc* 4(2), 232-43.

31 H. Aubin, J.W. Nichol, C. B. Hutson, H. Bae, A. L. Sieminski, D. M. Cropek, P. Akhyari, A. Khademhosseini **2010** *Biomaterials* 31(27), 6941-6951.

32 C.T. McKee, V. K. Raghunathan, P.F. Nealey, P. Russell, C. J. Murphy **2011** *Biophys J.* 101(9), 2139-46.

33 J. L. Charest, M. T. Eliason, A. J. García, W. P. King **2006** *Biomaterials* 27(11), 2487-94.